Recent Improvement of a Semi-Empirical Aeroacoustic Prediction Code for Wind Turbines

Patrick J. Moriarty*
National Renewable Energy Laboratory, Golden, CO 80401

Gianfranco Guidati†
Alstom Power Technology Center, Baden-Daettwil, Switzerland

and

Paul G. Migliore‡
National Renewable Energy Laboratory, Golden, CO 80401

Two improvements were made to a semi-empirical aeroacoustic prediction code for wind turbines. The first improvement involved modifying the turbulent inflow noise model. The original model, developed by Amiet was combined with a model created by Guidati and compared to two-dimensional airfoil noise measurements. The improved model accurately predicted the absolute and relative sound pressure level changes caused by angles of attack, Mach number, and airfoil shape. The second improvement to the code, was the replacement of the current semi-empirical boundary layer thickness prediction with a boundary layer prediction routine, XFOIL. Using direct boundary layer thickness calculations improved the prediction of turbulent boundary layer trailing edge noise for most airfoils over a frequency range of 1-4 kHz and angles of attack smaller than 5°. The boundary layer calculation method did not improve the estimation of laminar vortex shedding noise because of sensitivity of this noise source to boundary layer transition, which is not accurately modeled in the noise prediction code.

Nomenclature

B	=	stagnation enthalpy
b	=	airfoil span (m)
C	=	airfoil chord (m)
c	=	normalized speed of sound
c_o	=	speed of sound (m/s)
$\overline{D}$	=	directivity function
f	=	frequency (Hz)
He	=	Helmholtz number
I	=	turbulence intensity (%)
K	=	$2\pi f/U$ = wave number (1/m)
K_e	=	$3/(4L_{turb})$ = wave number range of energy-containing eddies (1/m)
$\overline{K}$	=	$K \cdot b/2$
$\hat{K}$	=	K/K_e
LFC	=	low-frequency correction factor
L_{turb}	=	turbulence length scale (m)
M	=	Mach number

* Research engineer, National Wind Technology Center, 1617 Cole Blvd., Golden, CO 80401, AIAA member.
† Research scientist, Segelhof 1, 5405 Baden-Daettwil, Switzerland
‡ Senior Project Leader, National Wind Technology Center, 1617 Cole Blvd., Golden, CO 80401, AIAA member.

R_{uu} = autocorrelation of longitudinal velocity
Re = Reynolds number based on chord
r_e = effective observer distance (m)
S = compressible Sears function
SPL = one-third octave band sound pressure level (dB)
St = fC/U_0 = Strouhal number
t = time (s)
U_0 = mean wind tunnel speed (m/s)
$\mathbf{U}$ = base flow velocity vector
$\boldsymbol{u}$ = total velocity vector
α = angle of attack (rad)
β^2 = $1\text{-}M^2$
δ^* = boundary layer displacement thickness (m)
δ = 99% boundary layer thickness (m)
ρ = normalized air density
ρ_o = air density (kg/m^3)
Φ = velocity potential
$\boldsymbol{\omega}$ = vorticity vector

I. Introduction

As wind turbines continue to proliferate globally and are placed close to population centers with restrictive noise ordinances, the amount of acoustic noise that a turbine radiates is becoming a crucial design driver for manufacturers. Currently, the tip speed of many wind turbine designs is limited by the amount of noise created by the blades passing through the atmosphere. Unfortunately, this limitation also caps the amount of energy capture for a specific design, which directly affects the cost of energy. To provide manufacturers with better information for designing future turbine configurations, the U.S. Department of Energy's National Renewable Energy Laboratory (NREL) has begun a comprehensive program involving development of more accurate acoustic measurement and prediction technologies.

One of these technologies is the development of a semi-empirical noise prediction code based on the works of Brooks, Pope, and Marcolini (BPM)[1] and Lowson.[2] This code models six different potential noise sources that are superimposed to estimate the total noise spectrum emitted from a wind turbine rotor. Each of these noise sources has a different physical method of noise generation that can be broken into two different categories: airfoil self-noise and turbulent inflow noise. Initial validation[3,4] of the semi-empirical prediction code revealed several areas for code improvement, which have been the focus of further study.

Researchers found the turbulent inflow noise to be the most questionable model in the semi-empirical code. During validation, this noise source dominated the total predicted noise spectrum for both two-dimensional airfoils and full-sized wind turbines, which was contrary to the results of previous researchers.[5] It was discovered that much of this error was due to the assumption that the airfoil sections along the turbine blades were modeled as flat plates, as in the work of Amiet.[6,7] This model resulted in much higher predicted noise levels than expected for airfoils with finite leading edge radii.

Another area of concern in the semi-empirical noise prediction code was the prediction of airfoil boundary layer properties. Many of the routines in the prediction code are based on the empirical formulae of Brooks, Pope, and Marcolini, who fit curves to experimental boundary layer thickness measurements of NACA 0012 airfoils. Because of this, the boundary layer properties for any airfoil calculated by the code are identical to the NACA 0012, meaning that differences in airfoil shape did not change predicted noise levels. During previous validation,[3,4] this resulted in large errors when comparing the effects of angle-of-attack on predicted noise for different airfoils.

In this study, researchers continue developing the semi-empirical noise prediction code by improving both the turbulent inflow and boundary layer prediction methods, allowing for different airfoil shapes to be modeled. Researchers modified the turbulent inflow noise model to incorporate the method of Guidati[8,9] that accurately estimates the effect of airfoil shape on turbulent inflow noise. After incorporating this correction, predicted results demonstrated the accepted theory that airfoils with larger leading edge radii produce less turbulent inflow noise.[10] Also, it was discovered that the basic assumptions used in the Lowson model were questionable. To resolve these questions, researchers replaced this model by the original model of Amiet,[7] which was considered more reliable.

To allow for predictions of the boundary layer properties of different airfoil shapes, a boundary layer prediction routine, XFOIL,[11] was incorporated into the aeroacoustic code. Using the surface coordinates of different airfoils as

inputs, the improved version of the code directly calculated the boundary layer properties for each of the different airfoil sections. These boundary layer properties were then used as inputs into the acoustic empirical relations of Brooks, Pope, and Marcolini.

While these improvements will eventually be incorporated into the full wind turbine noise prediction code, the results of this study are based on two-dimensional airfoils. The predictions from these improved routines are compared to the results from the original code and also to two-dimensional airfoil acoustic measurements made in a wind tunnel as described below.

II. Acoustic Measurements

The two-dimensional airfoil data were taken from a series of wind tunnel tests performed at NLR, the Netherlands National Aerospace Laboratory.[12,13] Acoustic noise spectra of several different airfoils were measured using a 48 microphone acoustic array. Details of the array, measurements, and data processing can be found in Refs. 12 and 13. It should be noted that using microphone array measurements to calculate absolute sound pressure levels is more computationally complex than measurements from a single microphone. The methods for absolute array measurements have recently been developed and are explained in detail in Ref. 14. Analysis of the acoustic array data provided one-third octave band sound pressure level measurements that could be directly compared to predictions given by the semi-empirical code.

In addition to a NACA 0012 airfoil, six different airfoils were tested in the NLR tunnel. These airfoils, shown in Figure 1, are commonly used in the wind turbine industry. The airfoils were tested over a range of angle of attack between 0° and ~8° (corrected for open jet effects). The range of tunnel speeds tested were for Reynolds numbers between 200,000 and 1 million. The chord lengths of all airfoils were 0.2286 m.

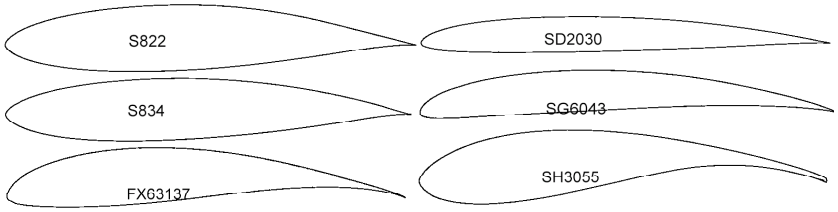

Figure 1. Six airfoil shapes tested in the NLR tunnel.

Each of the airfoils were tested with and without boundary layer tripping. When used, the boundary layer trips were strips of 11 mm wide (5% of the 0.2286 m chord) zigzag tape, placed at 2% chord on the upper surface and 5% chord on the lower surface near the leading edge. For most experimental conditions a trip thickness of 0.25 mm was used, except for Mach numbers of 0.066 and below, where the thickness was increased to 0.5 mm to ensure transition. This amount of tripping eliminated laminar boundary layer vortex shedding noise.

The airfoils were also tested for turbulent inflow noise, which required a highly turbulent inflow. As described in Ref. 12, the turbulent inflow was created by adding a wire mesh upstream of the test section. The mesh spacing was approximately 60 mm, which was assumed to be the dominant turbulence length scale[4] in the prediction calculation. The other parameter used for the turbulent inflow noise calculation is the turbulence intensity, which was measured to be approximately 9% in the empty test section. In the following sections, there are fewer measured data points for turbulent inflow noise than the other noise sources. This is because the turbulent grid created an extraneous high frequency noise source, and data above 3 kHz was deemed invalid.

III. Turbulent Inflow Modeling

To model the turbulent inflow noise, two different methods are combined to produce an estimate of the sound pressure level from this noise source. The first model is based on the work of Amiet,[6,7] who developed a first principles method for predicting turbulent inflow noise on airfoils. The major drawback to this method is that it assumes that the lift response of the airfoil to a turbulent inflow is the same as that for a flat plate, using linearized airfoil theory. This means that the influence of differences in airfoil shape on noise cannot be correctly modeled. The second method used in conjunction with Amiet's was one developed by Guidati[8,9] at the University of Stuttgart. This model does not predict absolute values, but is a relative correction to the flat plate model of Amiet that allows modeling of different airfoil shapes. More details of each method and comparisons to measured data are provided below.

A. Amiet model

The model of Amiet was developed from first principles and has been validated with some measurements of a NACA 0012 airfoil.[6,7] The model is composed of a high-frequency asymptote with a low-frequency correction. It is

necessary to model these two régimes separately because of their different flow physics. Low-frequency (or large length scale) turbulence will create changes in angle of attack and lift, leading to a dipole type noise source that will scale with M^6. High-frequency turbulence, on the other hand, behaves more like a turbulent boundary layer scattered near a sharp edge, which will scale closer to M^5. The following equations describe the basic formulation.

$$SPL_{Inflow} = SPL^{H}_{Inflow} + 10\log\left(\frac{LFC}{1+LFC}\right) \tag{1}$$

$$SPL^{H}_{Inflow} = 10\log\left(\rho_o^2 c_o^4 \frac{bL_{turb}}{2r_e^2} M^5 I^2 \frac{\hat{K}^3}{(1+\hat{K}^2)^{7/3}} \overline{D}\right) + 78.4 \tag{2}$$

$$LFC = 10S^2 M\overline{K}^2 \beta^{-2} \tag{3}$$

$$S^2 = \left(\frac{2\pi\overline{K}}{\beta^2} + \left(1 + 2.4\frac{\overline{K}}{\beta^2}\right)^{-1}\right)^{-1} \tag{4}$$

where each of these symbols is defined in the nomenclature section. Note that the constant in Equation 2 is different than that in Paterson and Amiet[7] because of the difference in units used for the density and speed of sound.

One of the important parameters in the above equations is the integral length scale of turbulence. Assuming Taylor's hypothesis of frozen turbulence, this length scale is defined by the following equation.

$$L_{turb} = U_0 \int_0^\infty R_{uu}(t)dt \tag{5}$$

Unfortunately, direct measurement of this length scale from the NLR measurements was not available in time for publication, and in all of the simulations it was assumed to be approximately 60 mm, the length scale of the mesh spacing.

As one can see in the above equations, the effect of angle of attack on turbulent inflow noise is not included. Previous studies[4,7] have shown that there is a small, but measurable effect on turbulent inflow noise. To correct for this minor effect, Paterson and Amiet proposed a slight correction to the low-frequency correction above.

$$LFC = 10S^2(1+9\alpha^2)M\overline{K}^2\beta^{-2} \tag{6}$$

where the angle of attack in this equation is measured in radians. Thus, for an angle of attack of 10° (0.17 radians) the contribution from this correction is approximately 1 dB, which is a small change.

Figure 2 shows the measured and predicted sound pressure level (SPL) for turbulent inflow noise of an S822 airfoil over a range of angle of attack and a Mach number of 0.095. In each of the following figures, the measured data in the plots are specified by symbols, whereas the predicted data are shown as lines of the same color. As suggested from the above formulation, there is a slight difference in the measured sound pressure levels when increasing the angle of attack. The prediction also calculates a slight increase in sound pressure level, but the absolute values as well as the relative change with angle of attack are not accurately reproduced. Also, the slope of the sound pressure level versus frequency is not accurately represented, with the measured levels falling off faster than the predicted. At a frequency near 2 kHz, the prediction overestimates the sound pressure level by 10 dB or more.

Figure 3 shows the turbulent inflow noise for the same airfoil over a range of Mach numbers at an angle of attack of 4.4°. Here the agreement between measured data and prediction is reasonable for the highest Mach number, but the accuracy of the prediction decreases as the Mach number decreases. This phenomenon was also observed by Amiet[6] who concluded that his method was more accurate as $Mb/L_{turb} \rightarrow \infty$. Thus, for a fixed airfoil span and turbulence length scale, the accuracy of the method will increase with Mach number. This conclusion also suggests that the method is more accurate when the turbulence length scale is significantly smaller than the span of the airfoil.

While the Amiet model produces reasonable results for some conditions, it is less accurate for others. An improvement to this model will be the addition of a correction developed by Guidati.

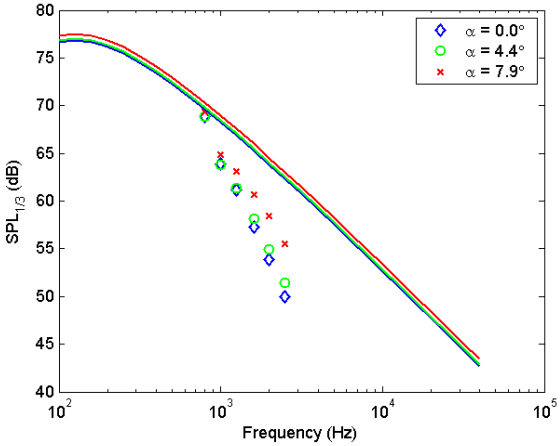

Figure 2. Turbulent inflow sound pressure level prediction using Amiet model and measured data for S822 at M = 0.095.

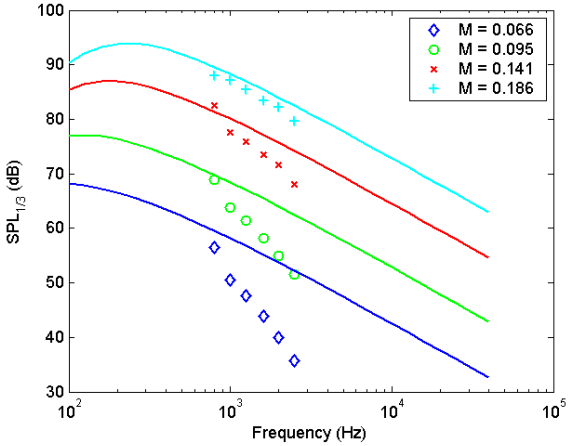

Figure 3. Turbulent inflow sound pressure level prediction using Amiet model and measured data for S822 at α = 4.4°.

B. Guidati model

1. *Basic equation*

The second model for inflow-turbulence noise allows calculation of the aerodynamic sound production that results from the interaction of vortical gusts with an isolated airfoil. The base flow around the airfoil is treated as an incompressible, inviscid potential flow. The vorticity is passively convected by the base flow. The sound generation is determined by the acoustic analogy proposed by Möhring[15]

$$\nabla \cdot (\rho \nabla B) - M_0^2 \rho \frac{D}{Dt}\left(\frac{1}{c^2}\frac{DB}{Dt}\right) = -\nabla \cdot (\rho \boldsymbol{\omega} \times \mathbf{u}) \qquad (7)$$

Here, B is the stagnation enthalpy, ρ the density and c the speed of sound of the base flow. The source term on the right-hand-side contains the vorticity $\boldsymbol{\omega}$ and the flow velocity $\boldsymbol{u}$. All quantities are non-dimensionalized by the velocity U_0 and density ρ_0 of the undisturbed base flow and by the airfoil chord C. This equation is simplified by assuming an incompressible base flow. Furthermore the velocity $\boldsymbol{u}$ is replaced by the base flow velocity $\mathbf{U}$ and the acoustic variable B and the vorticity $\boldsymbol{\omega}$ are considered to be harmonic with the $\exp(-i\,He\,t/M_0)$ convention and the Helmholtz number $He = fC/c_0$

$$\nabla^2 B + He^2 B + 2iHeM_0(\mathbf{U}\cdot\nabla)B = -\nabla\cdot(\boldsymbol{\omega}\times\mathbf{U}) \qquad (8)$$

This equation can be transformed with $B_i = Be^{iHeM_0\phi}$. This results in a Helmholtz equation for the transformed acoustic variable B_i which can be solved by using a boundary-element method, once the right-hand-side, i.e. the source term, is known:

$$\nabla^2 B_i + He^2 B_i = -\nabla\cdot(\boldsymbol{\omega}\times\mathbf{U})e^{iHeM_0\phi} \qquad (9)$$

2. Source term

Inflow turbulence noise results from the interaction of turbulence with an airfoil. As shown by Möhring's equation, vorticity is the property of the turbulence that is responsible for the sound production. An arbitrary turbulent flow field can be considered as a superposition of Fourier modes of vorticity with varying wave numbers and orientation angles. Here we consider harmonic disturbances, or gusts, which can be expressed by the following equation

$$\mathbf{u}_t = A\begin{pmatrix} -\tan\alpha \\ 1 \\ 0 \end{pmatrix} e^{iSt(x_1 + x_2 \tan\alpha)} \tag{10}$$

with the Strouhal number $St = fC/U_0$. The associated vorticity distribution is:

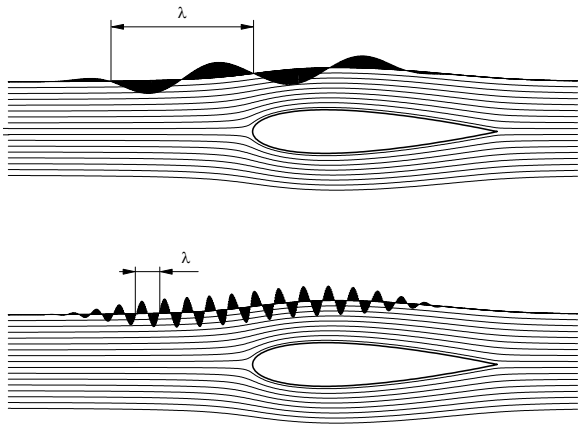

Figure 4. Discretization of vorticity field into harmonic vortex sheets.

$$\boldsymbol{\omega} = iStA\begin{pmatrix} 0 \\ 0 \\ 1+\tan^2\alpha \end{pmatrix} e^{iSt(x_1 + x_2 \tan\alpha)} \tag{11}$$

For practical reasons it is necessary to simplify the problem. First, this gust is split into a number of discrete sheets, which coincide with the streamlines of the mean flow around an airfoil. The vorticity, which is contained in the gust, is concentrated in these sheets. Figure 4 shows a schematic of the simplified method for two vorticity disturbances of differing wavelength.

This concentration results in vortex sheets that carry a harmonic distribution of vorticity. Mathematically, this is achieved through the use of delta functions. The discretization implies two parameters, the distance between two vortex sheets and the thickness of the stream that carries vorticity. Guidelines to determine these parameters have been formulated based on test simulations.

The second simplification is to limit the extent of the gust upstream and downstream of the airfoil. The starting point upstream is usually one chord length in front of the leading edge. Downstream of the leading edge the vorticity fades to zero before it reaches the trailing edge.

3. Prediction of Absolute Sound Spectra

The above model considers only simple harmonic disturbance patterns. The extension to actual sound levels is achieved in two steps. First, a number of different inclination angles are computed and combined energetically by assuming a von Karman spectrum. This is then compared to the sound produced by the same disturbances on a semi-infinite flat plate. The latter can be described in mathematically closed form by making use of the exact Greens function. This results in a frequency dependant correction of the sound level from a flat plate compared to an actual airfoil. This correction is finally applied to a prediction model for the absolute sound level of a flat plate airfoil as presented e.g. by Amiet. The final model is a combination of the Amiet model for determining the absolute level of sound pressure level and the Guidati model correction to the flat plate estimate.

After initial comparisons with measured data using the combined Amiet and Guidati model, a slight adjustment was made to greatly improve the accuracy of the model to predict absolute sound pressure levels. The adjustment was simply adding 10 dB, resulting in a final prediction method with the following formulation

$$SPL_{Inflow} = SPL_{Amiet} + SPL_{Guidati} + 10dB \tag{12}$$

Note that this 10 dB correction may only be applicable to the current data set and future research is required to determine if it is valid for more general use.

Figure 5 shows the predicted sound pressure levels from turbulent inflow noise for an S822 airfoil over the same range of angle of attack as in Figure 2. Note that the prediction was made only for the same range of frequencies as the measured data because of the added computational time required by the Guidati method. Nonetheless, agreement between measured and predicted sound pressure level is quite good, with the difference being less than 1 dB for most conditions. Also, unlike the Amiet method, the Guidati method accurately predicts the relative effects of angle of attack on the turbulent inflow noise.

Figure 6 shows a comparison between predicted and measured turbulent inflow noise for the same airfoil over a range of Mach numbers at an angle of attack of 4.4°. Again, the Guidati method predicts the total sound pressure level within 1-2 dB for most conditions.

Airfoil shape, or more specifically the leading edge radius of an airfoil greatly determines the amount of turbulent inflow noise an airfoil will radiate. It has been shown previously,[10] that the larger the leading edge radius of an airfoil, the quieter that airfoil will be for turbulent inflow noise. Each of the airfoils tested at the NLR varied greatly in camber, thickness, and also leading edge radius, as seen in Figure 1. Based on previous observations, one would expect that the SD2030 would radiate the most turbulent inflow noise, while the SH3055 would be the quietest. As shown in Figure 7, this is indeed the case, where the measured noise from the SH3055 is 8-10 dB quieter than the SD2030, depending on frequency. The other airfoils behave in a similar manner, depending on their leading edge radii.

Figure 8 shows the prediction of the turbulent inflow noise for each of these airfoils. Again, the agreement with measurement in both the absolute and relative sound pressure levels is fairly good, particularly for the thinnest airfoils. There is a slight disagreement with the measured values of Figure 7 for the relative magnitude of inflow noise from the S822, S834, and the FX63-137, but they are still within 2 dB of their measured values at lower frequencies. At the highest frequencies the difference between prediction and measurement is as high as 5 dB. Similarly, the agreement between measurement and prediction for the SH3055 airfoil is fairly good at lower frequencies, but decreases at higher frequencies where the difference is approximately 10 dB. This discrepancy at higher frequencies, which is also present in the previous two figures, will be the subject of further study. With this exception, the above results shows that the combination of the Amiet and Guidati model produces a promising prediction tool for turbulent inflow noise.

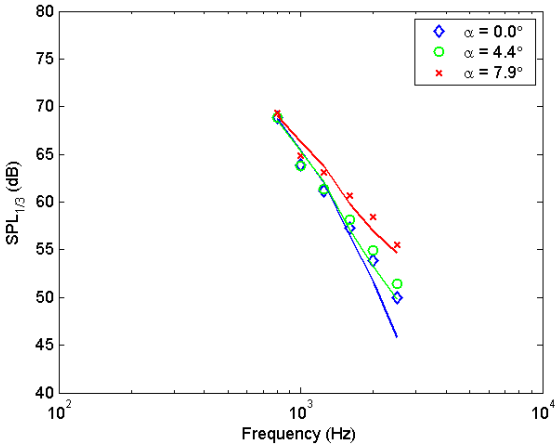

Figure 5. Turbulent inflow sound pressure level prediction using Guidati model and measured data for S822 at M = 0.095.

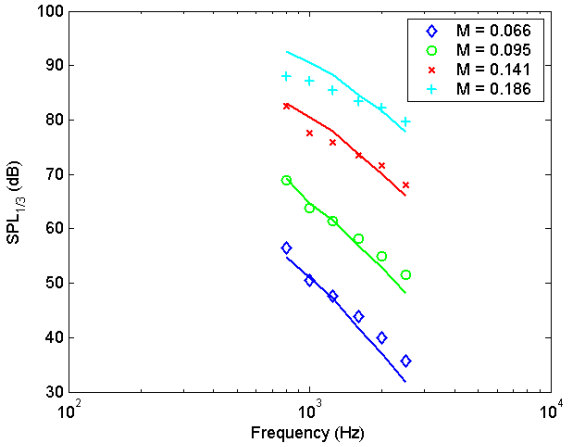

Figure 6. Turbulent inflow sound pressure level prediction using Guidati model and measured data for S822 at α = 4.4°.

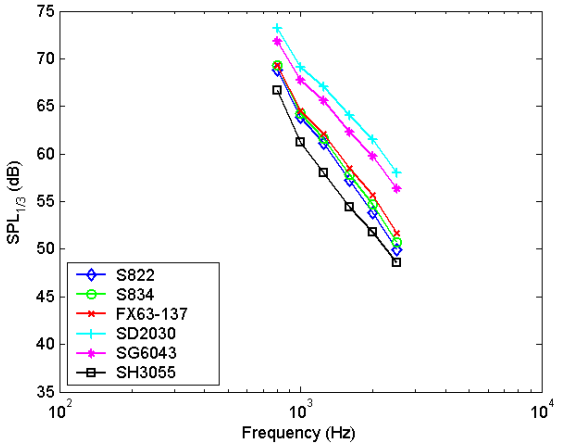

Figure 7. Measured turbulent inflow noise from all airfoils at M = 0.095 and α = 0°.

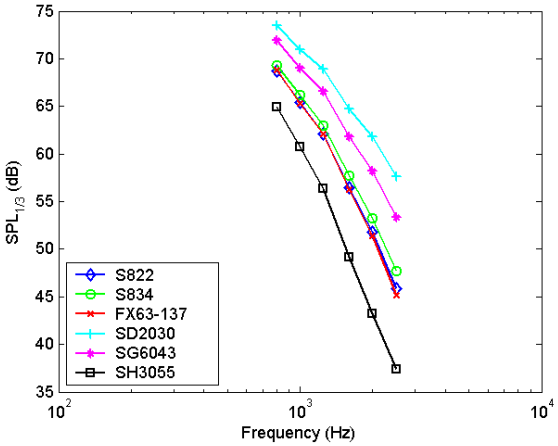

Figure 8. Predicted turbulent inflow noise from all airfoils at M = 0.095 and α = 0°.

IV. Boundary Layer Thickness

In the semi-empirical models of aeroacoustic noise, the boundary layer thickness is a critical parameter for determining the sound pressure level. Depending on the noise source, a different measure of boundary layer thickness is used in the empirical relationship. Because the measurements in the NLR tunnel were two-dimensional and the models had thin trailing edges, tip noise and blunt trailing-edge noise were considered negligible. In addition, without a turbulent grid in the tunnel, turbulent inflow noise was small, leaving only three noise mechanisms to model: turbulent boundary layer trailing-edge noise, separated flow noise, and laminar boundary layer vortex shedding noise. If the boundary layers of the airfoil were tripped, laminar boundary layer of noise could also be neglected. In the empirical models, it is assumed that for turbulent boundary layer and separated flow noise the sound pressure level is proportional to the following quantity

$$SPL_{TBL} \propto 10\log\left(M^5 \frac{\delta_s^* b}{r_e^2} \right) \tag{13}$$

where δ_s^* is the displacement thickness on the suction side of the airfoil. However, if the boundary layers of the airfoil are not tripped and the Reynolds numbers are sufficiently low, laminar vortex shedding noise can be prominent, which is similarly proportional to the following

$$SPL_{LBL} \propto 10\log\left(M^5 \frac{\delta_p b}{r_e^2} \right) \tag{14}$$

where δ_p is the 99% boundary layer thickness on the pressure side of the airfoil. Note that the difference in boundary layer parameter is the major difference between scaling laws of turbulent boundary layer noise and laminar boundary layer noise. The reasons for choosing these scaling parameters are described by Brooks, Pope, and Marcolini.[1]

As is also described in Brooks, Pope, and Marcolini, the semi-empirical models were created based on measurements of NACA 0012 airfoils. The disadvantage of these models is that they are unable to predict the effect of differing airfoil shape on acoustic noise because the boundary layer parameters are solely functions of Reynolds number and angle of attack. As an improvement to these models that will add the capability of predicting the effect of airfoil shape, an airfoil boundary layer prediction code is used to predict the boundary layer thicknesses, instead of the semi-empirical models. The boundary layer prediction code used was XFOIL, developed by Drela et al.[11] at the Massachusetts Institute of Technology. No modifications to the code were made, as a compiled version (v 6.94) was used in this study. Future research may require modifications to this code, but an initial study of this viability of this method does not.

In the following sections, both turbulent boundary layer noise and laminar boundary layer noise will be examined for three different airfoils of varying camber. The camber is considered an important parameter, because of its large influence on the boundary layer properties of an airfoil. The three airfoils from least to most amount of camber include (see Fig. 1): a NACA 0012, an S822, and an FX63-137. The airfoils also have different thicknesses, which will surely affect their boundary layer properties as well, but no attempt is made to separate the camber versus thickness effects. The effect of airfoil shape on a predicted sound pressure level using XFOIL will be compared to the original model as well as to experimental data from the NLR test.

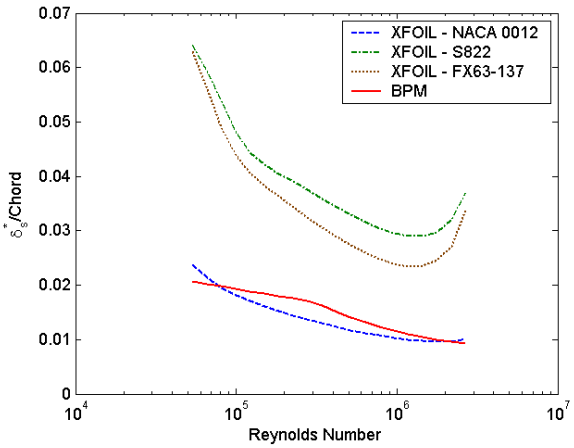

Figure 9. Tripped boundary layer displacement thickness at α = 4.4°.

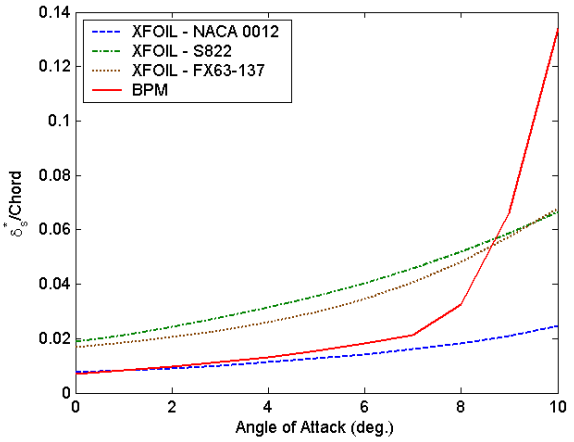

Figure 10. Tripped boundary layer displacement thickness at M = 0.095.

A. Tripped Boundary Layers

In the wind tunnel test, when the boundary layers were tripped, the turbulent boundary layer trailing-edge noise and separated flow noise were dominant. This was confirmed by a lack of tonal peaks in the sound pressure level spectra that are commonly present when there is laminar vortex shedding noise.

The thickness of the boundary layer and its condition (i.e. laminar or turbulent) are critical parameters for predicting airfoil noise. In the calculations using the original Brooks, Pope, and Marcolini model, the boundary layer of the airfoil was "lightly" tripped[1,4] by multiplying the calculated boundary layer thicknesses of the BPM by 0.6, as recommended in Ref. 1. This procedure is necessary because, in their experiments, Brooks, Pope, and Marcolini tripped their airfoils using 0.29 mm thick grit, covering the airfoil from the leading edge to 20% chord. This amount of tripping is believed to produce a thicker boundary layer than the current experiment. The calculated boundary layer thicknesses from XFOIL were used as is.

As shown in Eq. 13, the turbulent boundary layer noise models are proportional to the displacement thickness from the suction side of the airfoil. In the semi-empirical model of Brooks, Pope, and Marcolini, this boundary layer thickness is a function of both Reynolds number and angle of attack. Figure 9 shows the predicted displacement thicknesses as a function of Reynolds number using XFOIL for the three different airfoil shapes and also in the BPM model, which is the same for all airfoils. The angle of attack for these predictions was fixed at 4.4°. The prediction for the NACA 0012 airfoil using XFOIL is similar to the semi-empirical model of BPM over the range of Reynolds numbers with the largest difference of approximately 20% occurring near a Reynolds number of 300,000. The best agreement for this airfoil occurs at the highest and lowest Reynolds numbers. For the other two airfoils, the semi-empirical model dramatically underpredicts the boundary layer displacement thickness by as much as 300%. This is not unexpected as the other airfoils have larger amounts of camber, and therefore larger pressure gradients on the upper surface near the trailing edge. Notice in the XFOIL predictions at the highest Reynolds numbers, there is a dramatic increase in displacement thickness at the trailing edge for the two airfoils with large camber. This is caused by a small separation on the upper surface of the airfoil due to a large pressure gradient, which was not observed in the NACA 0012 airfoil predictions.

Figure 10 shows the predicted displacement thickness on the suction side of the airfoil for Mach number = 0.095 (Re = 500,000). Again, the agreement between XFOIL and BPM is a very good for the NACA 0012 at low angles of attack. BPM predicts thicknesses about half that of the other airfoils using XFOIL. As the angle of attack increases, however, the agreement between XFOIL and BPM becomes much worse, as the BPM model predicts separation at the trailing edge at lower angles of attack.

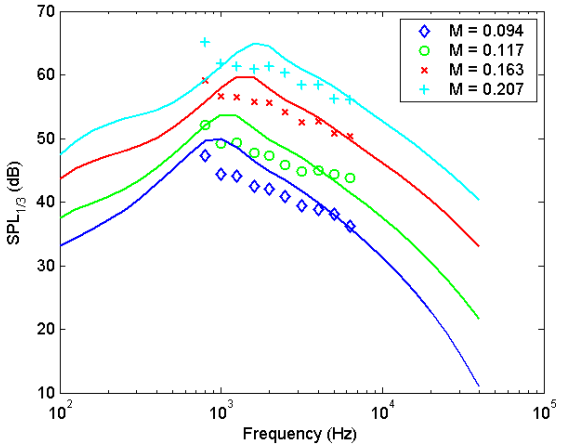

Figure 11. Tripped sound pressure level prediction using BPM and measured data for NACA 0012 at α = 4.0°.

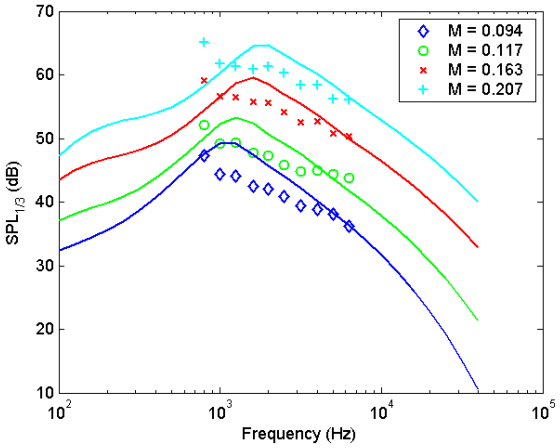

Figure 12. Tripped sound pressure level prediction using XFOIL and measured data for NACA 0012 at α = 4.0°.

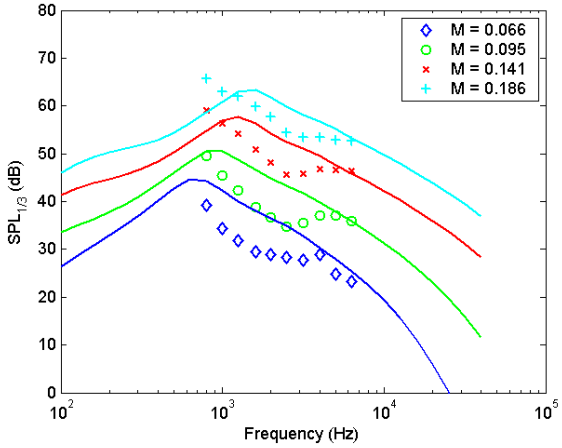

Figure 13. Tripped sound pressure level prediction using BPM and measured data for S822 at α = 4.4°.

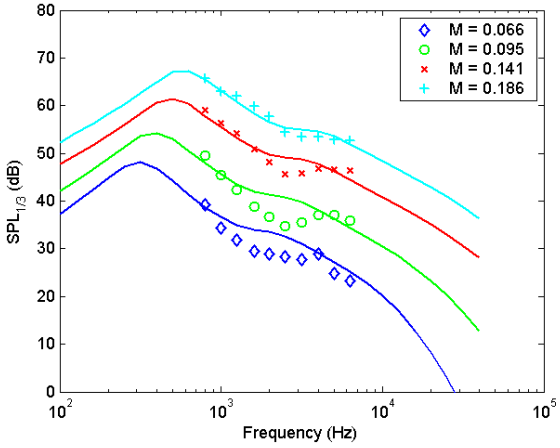

Figure 14. Tripped sound pressure level prediction using XFOIL and measured data for S822 at α = 4.4°.

Because of the differences in predicted displacement thicknesses, one would expect large differences in predicted sound pressure level except for the NACA 0012 airfoil at low angles of attack (below 6°). Figures 11 and 12 show the differences in prediction between XFOIL and the BPM model and also show the relative accuracy to the measured data. These plots are for a fixed angle of attack of 4.0° over a range of Mach numbers. As before, the measured data in each of the plots are specified by symbols, whereas the prediction methods are given by lines of the same color. The results from each of the prediction methods are fairly close, although the XFOIL method gives slightly lower predictions than BPM at the lowest Mach numbers. The XFOIL results are slightly closer to the data, but are not a dramatic improvement. Both methods give reasonable results for the absolute predictions, particularly at higher frequencies. Both methods also produce accurate relative trends in predicting the sound pressure level variation with Mach number. Similar agreement can be seen for the different angles of attack on this airfoil, although those results are not presented in this paper.

The differences in predicted sound pressure level between using XFOIL and the BPM model are more obvious in the two airfoils with significant camber and different thickness than the NACA 0012. Figures 13 and 14 show the predicted sound pressure levels and measured data for an S822 airfoil at an angle of attack of 4.4°. In the figure using the BPM semi-empirical model, one notices that the predicted results are similar to those of the NACA 0012 of Figure 11. However, using the XFOIL code to calculate the boundary layer properties produces improved results, with better agreement between the prediction and measured data over all frequencies. The agreement between measurement and prediction is especially good at the highest Mach number.

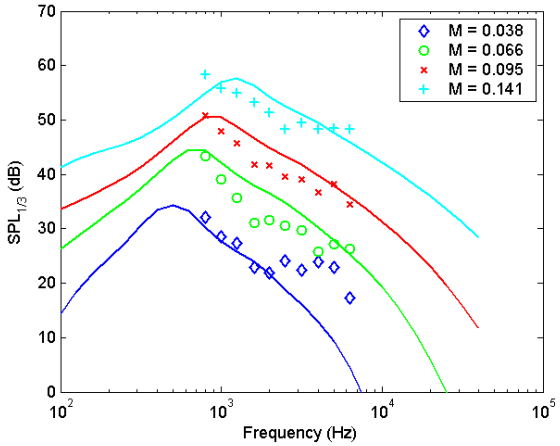

Figure 15. Tripped sound pressure level prediction using BPM and measured data for FX63-137 at $\alpha = 4.4°$.

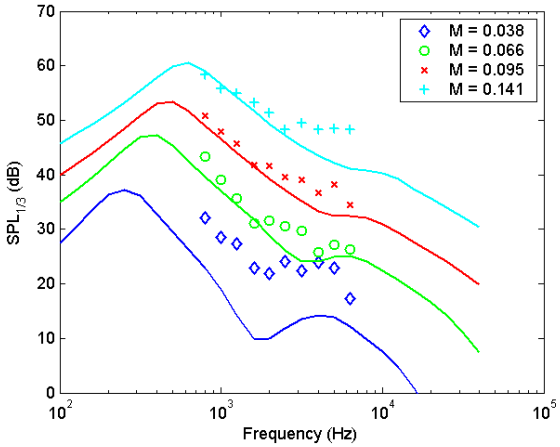

Figure 16. Tripped sound pressure level prediction using XFOIL and measured data for FX63-137 at $\alpha = 4.4°$.

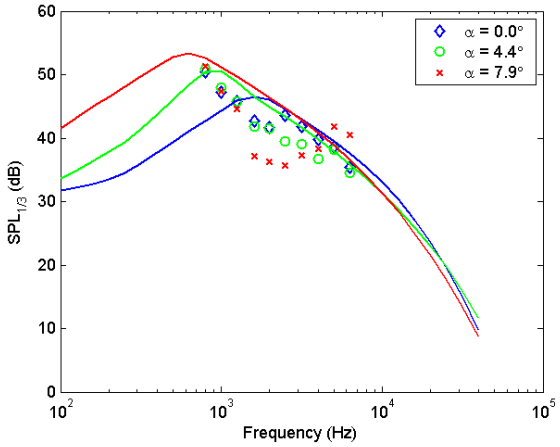

Figure 17. Tripped sound pressure level prediction using BPM and measured data for FX63-137 at M = 0.095.

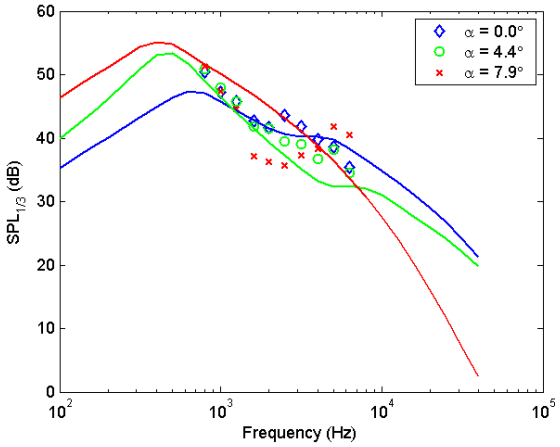

Figure 18. Tripped sound pressure level prediction using XFOIL and measured data for FX63-137 at M = 0.095.

Examining Figures 15 and 16, the results for the FX 63-137 airfoil are somewhat better when using XFOIL to predict the boundary layer thickness. However, the absolute levels at the lowest Mach number are underpredicted even though the relative shape of the spectrum is reproduced. This shape is not accurately predicted by the BPM model. Also notice that at the highest Mach number, the agreement between measurement and prediction at the highest frequencies is not as good for the XFOIL model, but the constant sound pressure level at these frequencies is also not predicted by the BPM model.

The last set of figures presented for tripped boundary layers are plots of the sound pressure level as a function of angle of attack for the FX 63-137 airfoil at a Mach number of 0.095. In Figure 17 notice that the BPM model does predict some change in sound pressure level at the lowest frequencies, but this is not consistent with the measured data. On the other hand in Figure 18, the XFOIL model does predict a change in sound pressure level in the mid-range of frequencies, between 1 kHz and 4 kHz. The shape is qualitatively consistent with the measured data, where the angle of attack reduces the sound pressure level in this mid-range, but the absolute values are still incorrect. Also, notice for the highest angle of attack a similar dip in the spectrum is not observed in the prediction but is in the measured data. The reason for the dip not being in the prediction is that separated-flow noise dominates at the highest angles of attack in the semi-empirical noise model, independent of the boundary layer thickness. Therefore, the shape is not changed by using the XFOIL boundary layer prediction method. Because this trend is not reproduced by the new model, further refinement of the semi-empirical model will be necessary to adjust the separated flowed noise to account for different airfoil shapes.

B. Natural Transition Boundary Layers

Often in the design of wind turbines, the airfoils along the blades are not tripped and a transition to turbulence may not occur until near the trailing edge of the airfoil. This may be true for smaller wind turbines and at inboard stations of the blade where the Reynolds numbers are small and laminar flow could potentially exist. If laminar flow does exist, it could produce an acoustic noise source that is physically different than that of turbulent boundary layer and separated flowed noise. This noise source involves a feedback loop of coherent vortices or small laminar separation bubbles near the trailing edge on the pressure side of the airfoil feeding back to the upper surface transition point. This feedback creates a tonal amplification that has been observed in two-dimensional wind tunnel tests. It is unclear whether this phenomenon actually occurs on wind turbines, since they often operate in very turbulent conditions where laminar flow will not likely exist. However, the laminar vortex shedding noise model was retained in the code and the effect of using the improved XFOIL model for boundary layer thickness prediction was examined.

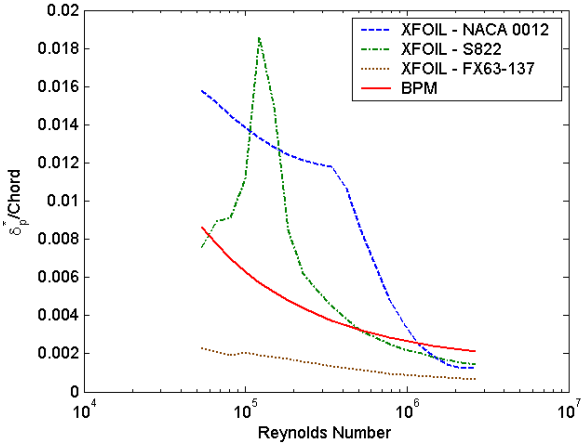

Figure 19. Untripped boundary layer displacement thickness at α = 4.4°.

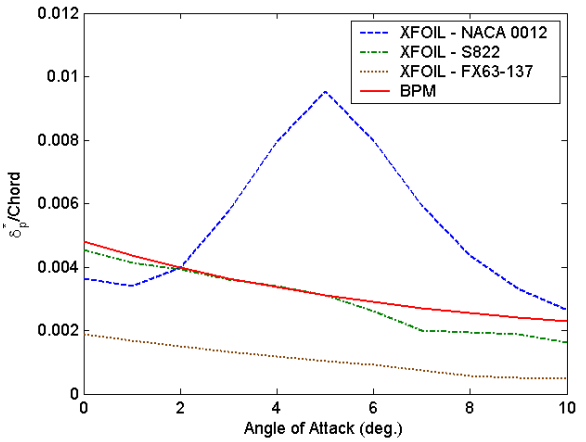

Figure 20. Untripped boundary layer displacement thickness at M = 0.095.

As described in Brooks, Pope, and Marcolini,[1] the important boundary layer parameter for laminar vortex shedding noise is the boundary layer thickness on the pressure side of the airfoil. The boundary layer thickness used in the model is not the displacement thicknesses, as used in a turbulent boundary layer noise models, but is the 99% velocity boundary layer thickness, defined as the distance from the airfoil where the velocity reaches 99% of the local "freestream" velocity. Unfortunately, the compiled version of XFOIL does not output this boundary layer thickness,[11] even though it is internally calculated. Instead, researchers calculated the displacement thickness on the pressure side of the airfoil with XFOIL and used a semi-empirical relationship from Brooks, Pope, and Marcolini to determine the 99% boundary layer thickness to input into the noise model. The relationship used to calculate the 99% boundary layer thickness from the displacement thickness was created by combining equations 5 and 6 in Ref. 1. This relationship is solely a function of the Reynolds number, Re.

$$\frac{\delta_p}{\delta_p^*} = 10^{\left[-1.3618+0.6352\log_{10}(\mathrm{Re})-0.0463(\log_{10}(\mathrm{Re}))^2\right]} \tag{15}$$

In Ref. 1 there is also a slight dependence on angle of attack, but it was shown that for the highest angle of attack in the study, 7.9°, this dependence only changed the boundary layer thickness value by 2%. With this equation, we can use the displacement thickness calculated in XFOIL as an input to the noise models without drastically changing the empirical model itself. Of course, the relationship between 99% boundary layer thickness and the displacement thickness will remain fixed to the empirical model based on a NACA 0012. This relationship will surely be different for airfoils with different shape and pressure distributions, but as will be shown, the boundary layer thickness is not always the most important parameter for laminar vortex shedding noise.

Figures 19 and 20 show the calculated displacement thickness on the pressure side of the airfoils, using the XFOIL routine and the semi-empirical BPM model, over a range of Reynolds numbers and angles of attack. Notice the large variations in the predicted displacement thickness values in the figures. Unlike the tripped boundary layer predictions, the untripped boundary layer thickness predictions for the NACA 0012 are very different between the

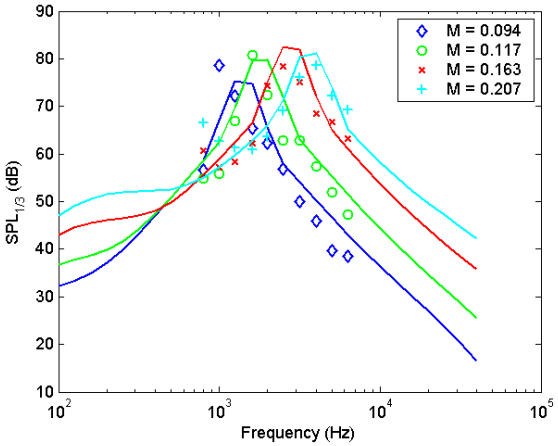

Figure 21. Untripped sound pressure level prediction using BPM and measured data for NACA 0012 at α = 4.0°.

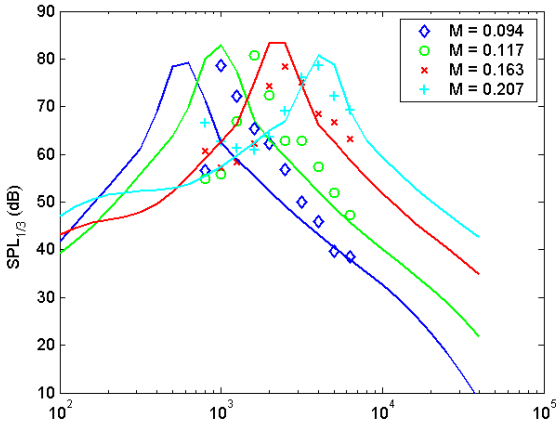

Figure 22. Untripped sound pressure level prediction using XFOIL and measured data for NACA 0012 at α = 4.0°.

XFOIL method and the BPM method. For a midrange angle of attack around 5° in Figure 20, the difference is over 100%. Further inspection showed that the much larger prediction by XFOIL was caused by a separation bubble on the lower surface of the airfoil whose size varies with angle of attack. This separation bubble was not observed in the experiments of BPM and the measured boundary layer thickness was much smaller. For naturally transitioning boundary layers, the predicted or measured trailing edge boundary layer thickness is very sensitive to transition location. So, these large variations are not surprising. In the calculations, XFOIL uses a transition criteria based on an e^n model where the constant n is equal to 9, a typical value for generic wind tunnels. The transition locations on which the BPM model is based are unknown.

The predicted boundary layer thickness will also vary greatly with Reynolds number as shown by calculations of the NACA 0012 and S822 airfoils in Figure 19. As Reynolds numbers increase, the displacement thickness decreases and seems to asymptotically approach a more consistent value. These values are still much different than those predicted by the BPM model. The predicted displacement thickness for the NACA 0012 and S822 only agree over a certain range of Reynolds number and angle of attack, while the BPM model consistently overpredicts the XFOIL result for the FX 63-137. One would expect that this would result in extremely different sound pressure level predictions, as will be shown below.

Figures 21 and 22 show predictions of sound pressure level using the two boundary layer prediction methods for a NACA 0012 airfoil at an angle of attack of 4°. Also presented in the figures are the measured data from the NLR wind tunnel test. Note that the BPM model gives excellent agreement with the measured data over the range of Mach numbers, while the XFOIL boundary layer prediction produces similar results at the highest Mach numbers, but the accuracy of the prediction decreases with tunnel speed. This is consistent with comparisons of Figures 19 and 20, where the displacement thickness only agrees for certain operating conditions.

When adding slightly more camber to the airfoil, as with the S822, the agreement between prediction (using either method) and the measured data becomes much worse. Figures 23 and 24 show the measurements and predictions of sound pressure level for an S822 at an angle of attack of 4.4°. Interestingly, both the XFOIL model and BPM model predict very similar spectra at these conditions. This is because, as seen in Figure 19, the predicted boundary layer thicknesses are fairly close over this range of Reynolds numbers. However, the amplitudes and shapes present in the measured data are not accurately estimated. Close examination of the measured data, reveals that there are small (5 dB) peaks from laminar vortex shedding on the airfoil, that change frequency with Mach number. The frequencies of these peaks are accurately estimated by the semi-empirical code, but the amplitudes of these peaks are overestimated by 20 dB or more. For this airfoil, the laminar vortex shedding is an important feature of the noise, but it does not dominate the spectra as with the NACA 0012 airfoil.

With even more camber in the airfoil, the FX 63-137 has even less influence on laminar vortex shedding in the measured noise spectra, as seen in Figures 25 and 26. In these measured spectra, the only visible peaks are slight rises in the sound pressure level at the highest frequencies, which may or may not be due to laminar vortex shedding. On the other hand, the prediction methods produce large peaks that greatly overestimate the measured levels, except at the lowest Mach number of 0.038. The frequencies of the predicted peaks are also quite different between the two boundary layer prediction methods, as would be expected from the results of Figures 19 and 20.

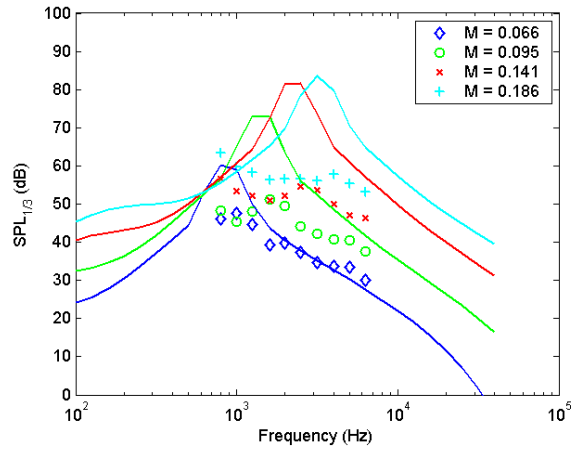

Figure 23. Untripped sound pressure level prediction using BPM and measured data for S822 at α = 4.4°.

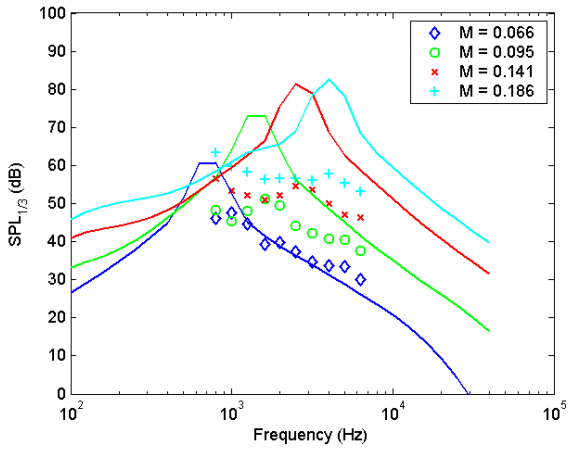

Figure 24. Untripped sound pressure level prediction using XFOIL and measured data for S822 at α = 4.4°.

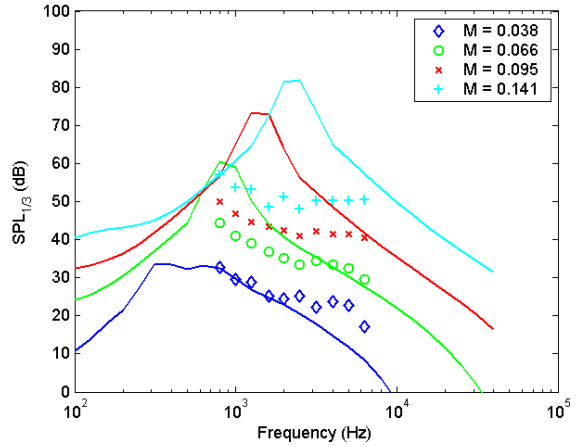

Figure 25. Untripped sound pressure level prediction using BPM and measured data for FX63-137 at α = 4.4°.

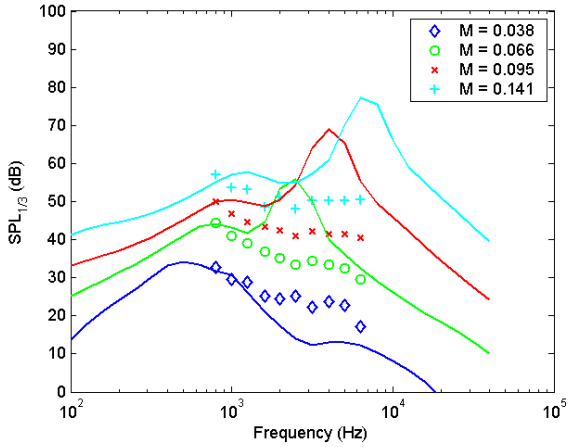

Figure 26. Untripped sound pressure level prediction using XFOIL and measured data for FX63-137 at α = 4.4°.

This discrepancy between measurement and prediction indicates that the physical basis of the semi-empirical model is not valid for higher camber (and/or thickness) airfoils. Perhaps this is because the laminar vortex shedding noise is suppressed by increased turbulence over the upper surface of the airfoil, caused by a larger pressure gradient due to increased camber. The laminar vortex shedding noise is also known to be sensitive other variables, such as trailing-edge geometry, the effects of which require further study.

The final sets of figures for this section are also for the FX 63-137 airfoil and examine the effect of angle of attack at a Mach number of 0.095. Figures 27 and 28 show the results from the XFOIL and the BPM methods for three different angles, as well as measured data. Note that for the zero angle of attack case, there is a slight peek in the measured data from laminar vortex shedding around 2 kHz. Both boundary layer methods give a reasonable estimate of the amplitude of this peak, but do not accurately predict its frequency. For the two higher angles of attack, any sign of laminar vortex shedding noise in the measured spectrum has vanished. For an angle of attack of 4.4°, both prediction methods calculate large laminar vortex shedding peaks, which are not present in the measured data. At the highest angle of attack, the predicted spectra lose this peak, indicating that separating flow noise is now the dominant source. These calculated spectra are in better agreement than the 4.4° case, although differences of 5 dB are observed for most frequencies. The observations made from these plots suggest that a beneficial way to change the semi-empirical noise calculations for different shaped airfoils should include methods to relate airfoil camber and thickness to the angle in which separated flow noise will dominate.

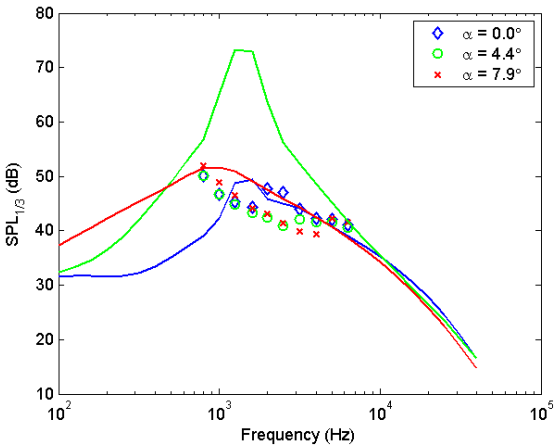

Figure 27. Untripped sound pressure level prediction using BPM and measured data for FX63-137 at M = 0.095.

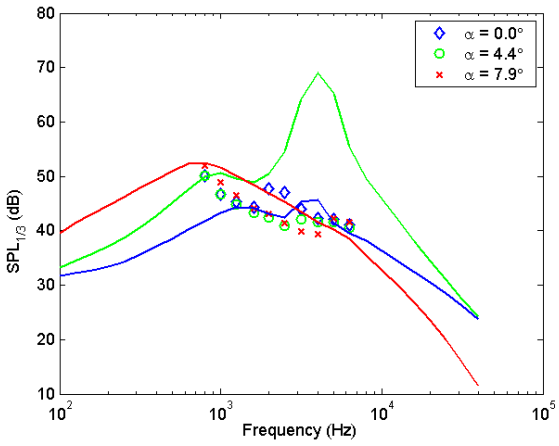

Figure 28. Untripped sound pressure level prediction using XFOIL and measured data for FX63-137 at M = 0.095.

V. Conclusion

Combination of the Amiet model with the Guidati model resulted in an excellent prediction method for turbulent inflow noise on airfoils. This method accurately reproduced absolute and relative sound pressure level values for changes in angle of attack, Mach number, and airfoil shape. This method will greatly improve the prediction capability for this noise source on wind turbines.

The use of a more accurate boundary layer prediction code, XFOIL, for the prediction of turbulent boundary layer trailing edge noise was also fairly successful. Using boundary layer thicknesses that were directly calculated, instead of the existing semi-empirical model, improved the prediction of sound pressure level for most airfoil shapes over a range of frequencies between 1-4 kHz. The improvement was most obvious between 0° and approximately 5° angle of attack, because at higher angles of attack separated flow noise dominated the acoustic spectra and was less dependent on the boundary layer thickness parameter.

Using the boundary layer thickness code in the laminar vortex shedding noise routine did not greatly improve the prediction of this noise source. This lack of improvement is attributed to the sensitivity of this noise source to the transition of the boundary layer on the upper and lower surfaces of the airfoil, whose locations and effects on the flow field are difficult to predict. Further changes to this noise module will be necessary to be able to predict sound pressure levels of airfoils with shapes significantly different than a NACA 0012.

References

[1]Brooks, T.F., Pope, D.S., and Marcolini, M.A., "Airfoil Self-Noise and Prediction," NASA Reference Publication 1218, National Aeronautics and Space Administration, 1989.

[2]Lowson, M.V., "Assessment and Prediction of Wind Turbine Noise," ETSU W/13/00284/REP, 1993.

[3]Moriarty, P.J. "Development and validation of a semi-empirical wind turbine aeroacoustic code," *Proc., 2004 ASME Wind Energy Symposium*, 42nd AIAA Aero. Sci. Mtg., AIAA2004-1189, 2004.

[4]Moriarty, P.J. and Migliore, P., *Semi-Empirical Aeroacoustic Noise Prediction Code for Wind Turbines*, NREL/TP-500-34478, National Renewable Energy Laboratory, Golden, CO, 2003.

[5]Fuglsang, P., Madsen, H.A., *Implementation and Verification of an Aeroacoustic Noise Prediction Model for Wind Turbines*, Risø-R-867(EN), Risø National Laboratory, Roskilde, Denmark, 1996.

[6]Amiet, R.K., "Acoustic Radiation from an Airfoil in a Turbulent Stream," J. Sound Vibration, Vol. 41, No. 4**,** pp. 407-420, 1975.

[7]Paterson, R.W., Amiet, R.K., "Acoustic Radiation and Surface Pressure Characteristics of an Airfoil Due to Incident Turbulence," NASA CR-2733, National Aeronautics and Space Administration, USA, September, 1976.

[8]Guidati, G., Dassen, T., Parchen, R., Bareiß, R., Wagner, S., "Simulation and Measurement of Inflow-Turbulence Noise on Airfoils," AIAA Paper 97-1698, 1997.

[9]Guidati, G., Wagner, S., "Simulation of Aerodynamic Sound Generation on Airfoils in Low Mach-Number Flows," *Proc., Fifth International Congress on Sound and Vibration*, Adelaide, Australia, 1997.

[10]Wagner, S., Bareiß, R. and Guidati, G., *Wind Turbine Noise*, Springer-Verlag, Berlin, 1996.

[11]Drela, M. and Youngren, H.. *XFOIL 6.94 User Guide*, Massachusetts Institute of Technology, Cambridge, Massachusetts, 2001.

[12]Oerlemans, S., *Wind Tunnel Aeroacoustic Tests of Six Airfoils for Use on Small Wind Turbines*, National Aerospace Laboratory, Emmeloord, The Netherlands, NREL SR-500-34470, 2003.
[13]Migliore, P.J. and Oerlemans, S., "Wind Tunnel Aeroacoustic Tests of Six Airfoils for Use on Small Wind Turbines," AIAA 2004-1186, to be presented at the 42nd AIAA Aero. Sci. Mtg, 2004.
[14]Sijtsma, P., "Calculating Absolute Source Powers from Phased Arrady Measurements," NLR-CR-2002-358, National Aerospace Laboratory, Emmeloord, The Netherlands, 2002.
[15]Möhring, W., "Modeling Low Mach-Number Noise," in *Mechanics of Sound Generation in Flows*, Müller, E.A. (Editor), Springer Verlag, 1979.